Physica D 68 (1993) 299–317
North-Holland

SDI: 0167-2789(93)E0204-0

PHYSICA D

Chaotic traveling waves in a coupled map lattice

Kunihiko Kaneko[1]

Department of Pure and Applied Sciences, College of Arts and Sciences, University of Tokyo, Komaba, Meguro-ku, Tokyo 153, Japan

Received 11 December 1992
Revised manuscript received 30 April 1993
Accepted 4 May 1993
Communicated by A.V. Holden

Traveling waves triggered by a phase slip are studied in a coupled map lattice. A local phase slip affects globally the system, which is in strong contrast with kink propagation. Attractors with different velocities coexist, and form quantized bands determined by the number of phase slips. If the system size is not far from an integer multiple of the selected wavelength, attractors are tori; otherwise, weak chaos induces modulation of waves or a chaotic itinerancy of traveling states, with a long-ranged temporal correlation. Supertransients before the formation of traveling waves are noted in the high nonlinearity regime. In the weaker nonlinearity there are fluctuations of domain sizes and Brownian-like motion of domains. Propagation of chaotic domains by phase slips is also found.

1. Introduction

The coupled map lattice (CML) is a dynamical system with discrete time ("map"), discrete space ("lattice"), and a continuous state. It usually consists of dynamical elements on a lattice interacting ("coupled") among suitably chosen sets of other elements [1–17][#1]. The CML was originally proposed as a simple model for spatiotemporal chaos; high-dimensional chaos involving spatial pattern dynamics.

Modeling through a CML is carried out as follows: Choose essential procedures which are essential for the spatially extended dynamics, and then replace each procedure by a parallel dynamics on a lattice. The CML dynamics is obtained by successive application of each procedure. As an example, assume that you have a phenomenon, created by a local chaotic process and diffusion. Examples can be seen in convection, chemical turbulence, and so on. In the CML approach, we reduce the phenomena into local chaos and diffusion processes. If we choose a logistic map $x'_x(i) = f(x_n(i))$ $(f(y) = 1 - ay^2)$ to represent chaos, and a discrete Laplacian operator for the diffusion, our CML is given by

$$x_{n+1}(i) = (1-\epsilon)f(x_n(i)) + \tfrac{1}{2}\epsilon f(x_n(i+1)) + f(x_n(i-1)) \qquad (1)$$

Here a is the parameter for the nonlinearity, while ϵ is the coupling representing the diffusion strength. One of the merits of the CML approach lies in its prediction of novel qualitative classes of behavior that are found generally irrespective of the details of the model. Classes discovered thus far include spatial bifurcation, frozen random chaos, pattern selection with suppression of chaos, spatiotemporal intermit-

[1] E-mail address: chaos@tansei.cc.u-tokyo.ac.jp.

[#1] For type-I spatiotemporal intermittency, see [1,6], and [9]. For type-II intermittency, see [10]; see also [11].

0167-2789/93/$06.00 © 1993 – Elsevier Science Publishers B.V. All rights reserved

tency, soliton turbulence, and quasistationary supertransients [2–7].

Here we report a novel universality class in CML, which is related to recent experiments in fluid convection and liquid crystals: (chaotic) traveling waves. We study the qualitative and quantitative nature of the chaotic traveling wave, with the help of the Lyapunov analysis and co-moving mutual information flow.

In our model (1), the observed domain structures are temporally frozen when the coupling ϵ is small (<0.45) [5]. For larger couplings, domain structures are no longer fixed in space, but can move with some velocity. For weak nonlinearity ($a < a_{ps} \approx 1.55$), the motion of a domain is rather irregular and Brownian-like, while pattern selection yielding regular waves is found for larger values of the nonlinearity ($a > a_{ps} \approx 1.55$). These two regions correspond to the frozen random phase and (frozen) pattern selection in the weaker coupling regime [5], respectively. Our novel discovery here is of non-frozen patterns that can slowly move.

The traveling wave here is sustained by phase slips, which are localized objects with 2π phase advance of oscillation. We have found that the velocity of the wave is proportional to the number of phase slips. This additivity of the velocity is in strong contrast with soliton type propagation, and will be studied in detail.

For most parameter regimes with $a > a_{ps}$ the motion of the traveling wave is quasiperiodic, unless there is a mismatch between the size and the wavelength. In the latter case we have seen chaotic itinerancy among traveling states with different velocities. If a is larger than $a_{tr} \approx 1.74$, we have observed quasistationary chaotic transients before the system is attracted to regular traveling wave. The length of transient diverges with the system size. In the transient state the motion is fully chaotic.

The phase diagram for the strong coupling regime is shown in table 1. The diagram is essentially independent of ϵ for $\epsilon > 0.45$, except weak dependence of a_{tr} on ϵ, and the increase of the wavelength of the selected pattern with ϵ.

The organization of the paper is as follows. In section 2, the coexistence of traveling-wave attractors with different velocities is shown. The quantization of selected velocities is noted. The mechanism of traveling is attributed to the existence of phase slips, as studied in detail in section 3. In section 4, detailed studies of the basin volume for the traveling attractors and the parameter-dependence of velocities are given. The traveling wave suppresses chaos almost completely, as is confirmed by the Lyapunov analysis in section 5. When the size is not close to an integer multiple of the selected wavelength, weak chaos remains, which leads to the modulation of traveling wave or a chaotic itinerancy over different traveling wave states due to chaotic frustration in the pattern. The long-term correlation of the itinerancy is studied in section 6. The flow of information in the traveling wave is characterized by co-moving mutual information flow in section 7. Quasistationary supertransients before falling on a traveling wave attractor are studied in section 8. Switching among attractors by a local input is studied in section 9, where

Table 1
Phase diagram for our CML, with $\epsilon > 0.45$.

a	1.4011 ... ↓	a_{ps}(~1.55 ...) ↓	a_{tr}(~1.74) ↓	
Moving kink in period-doubling media	Wandering domain by frozen chaos	Traveling wave by phase slip (pattern selection) without long transients		supertransient

it is shown that a single input can induce a transition of an attractor's velocity and thus affect the entire lattice. In a weak nonlinearity regime, the motion of a domain is no longer regular. The Brownian-like motion of domains is studied in section 10. If the local dynamics is not chaotic, but periodic with period 2^n, we can have traveling kinks in the strong coupling regime. These kinks are localized in space and do not have a global influence, in contrast with the phase slips, as will be shown in section 11. Discussions and a summary are given in section 12 [1].

2. Selection of discrete velocities

In the CML (1), only a few patterns with some wavenumbers are selected for large nonlinearity ($a > 1.55$ for $\epsilon = 0.5$). Besides the non-traveling pattern, there are moving patterns which form a traveling wave, as shown in fig. 1a (see also [1]). We note that such traveling attractors are not observed in the weak coupling regime ($\epsilon < 0.4$). The selected velocities of the attractors in the examples are rather low, in the order of 10^{-3}, and attractors with different velocities of waves coexist. In the simulation, the admissible velocities v_p for the attractors lie only in narrow bands located at $\pm v_1, \pm v_2, \ldots, \pm v_k$ (e.g., $0.8v_k < v_p < 1.2v_k$). For example, $v_1 = 0.95 \times 10^{-4}$, $v_2 = 1.9 \times 10^{-3}$, and $v_3 = 2.9 \times 10^{-3}$, $v_4 = 3.9 \times 10^{-3}$, for $a = 1.72$, $\epsilon = 0.5$, and $N = 100$. No attractors exist with $v_p \approx 0$ but $v_p \neq 0$. Between neighboring velocity bands there is a clear gap where no attractors exist with such velocity. For all parameters, v_k is approximately proportional to k.

One might argue that this discreteness of the velocity bands may be an artifact of our model, which is discrete in both space and time. Since the speed is very slow (i.e., the order of 10^{-3} site per step), it is not easy to imagine a mechanism to which our original discreteness (the order of 1 site per step) is relevant. To examine possible

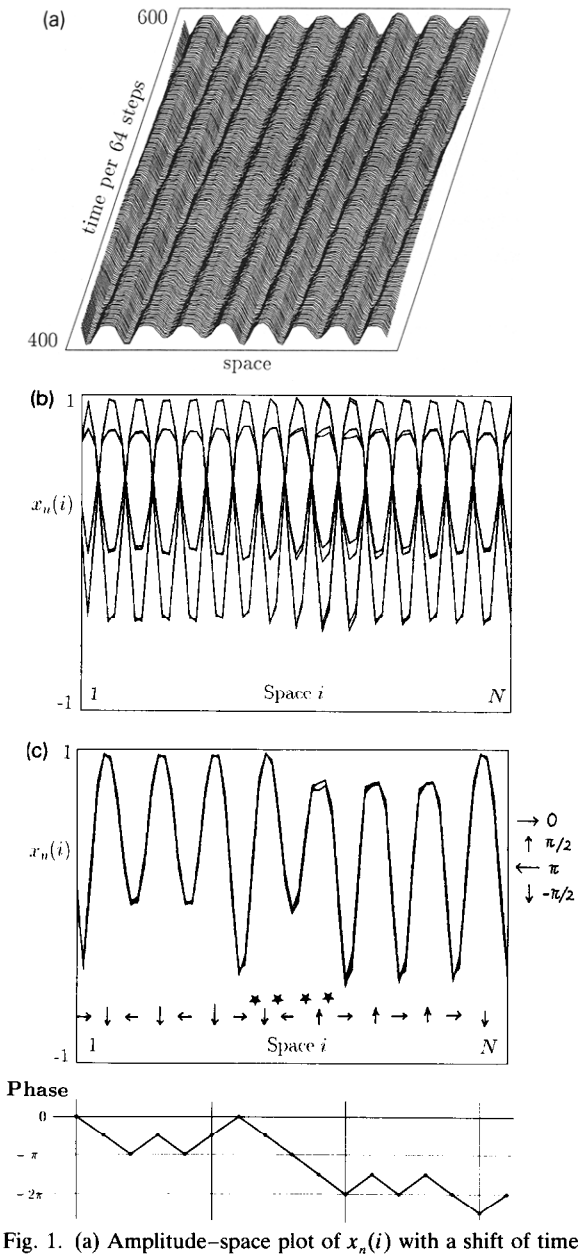

Fig. 1. (a) Amplitude–space plot of $x_n(i)$ with a shift of time steps. 200 sequential patterns $x_n(i)$ are displayed with time (per 64 time steps), after discarding 25 600 initial transients, starting from a random initial condition. $a = 1.71$, $\epsilon = 0.5$, and $N = 64$. An example of an attractor with $v_p = v_1$. (b) Space–amplitude plot of $x_n(i)$. $a = 1.72$, $\epsilon = 0.5$, and $N = 64$. 100 steps are overlaid after discarding 10 000 initial transients. This wave pattern is traveling to the left direction. (c) The same plot, shown per 4 steps. Arrows indicate the phase of oscillation of the corresponding domains. The bottom figure shows the phase of oscillation of the corresponding domain, measured from the site $i = 1$.

effects of the spatial discreteness, we have also simulated a CML with a much longer coupling range, following the method of Section 7.5 in [5]; i.e., a repetition of the diffusion procedure in the CML of I_D times per local nonlinear mapping procedure. With the increase of I_D, the range of the diffusion is increased, making our attractor spatially much smoother, approaching a continuous space limit. Our traveling attractors have then much longer wavelengths, and have higher quantized speeds. For example the speed band at v_1 is amplified roughly 4 times by choosing $I_D = 8$ (for $a = 1.72$, $\epsilon = 0.5$, $N = 200$). Thus the discreteness in space is not relevant to the discrete selection of velocities.

The wavelength of a pattern is almost independent of the velocity of an attractor. The velocity is governed not by the (spatial) frequency but by the form of the wave. Since our model has mirror symmetry, a traveling wave attractor must break the spatial symmetry. The wave form is spatially asymmetric. Here this spatial (a)symmetry is not a local property. Indeed, the waveform differs by domains of unit wavelength. The asymmetry is defined only through the average over the total lattice. We have measured the spatial asymmetry by

$$s \equiv \left\langle \frac{1}{N} \sum_{j=1}^{N} [x_n(j+1) - x_n(j)]^3 \right\rangle \qquad (2)$$

with the long time average $\langle \cdots \rangle$. This third power is chosen just because it is the simplest moment of an odd power, since the first power $\Sigma_{j=1}^{N} [x_n(j+1) - x_n(j)]$ vanishes due to the periodic boundary conditions.

In the present paper the velocity of an attractor is estimated by the following algorithm: Find the minimum k such that $\Sigma_{j=1}^{N} [x_{n+2m}(j) - x_n(j-k)]^2$ is a minimum. Up to some value of $2m$, the minimum is found for the lattice displacement $k = 0$. If the attractor is moving, at a certain delay $2m$, the minimum is not obtained for $k = 0$, but for $k = \pm 1$. With the help of this delay the speed of the pattern is estimated as $\pm 1/2m$. In fig. 2, we have measured the above $2m$ over time

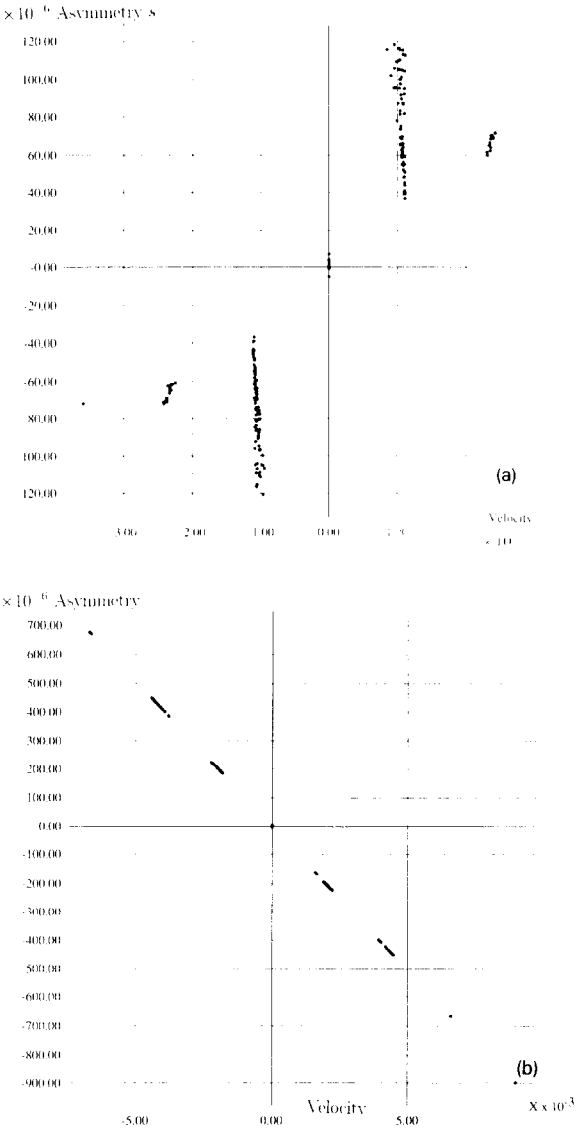

Fig. 2. Asymmetry s versus velocity v_p for attractors started from randomly chosen 300 initial conditions. The asymmetry and velocity are computed from the average of 160 000 steps after discarding 100 000 initial transients. $N = 64$ and $\epsilon = 0.5$. (a) $a = 1.69$, (b) $a = 1.8$.

160 000 steps, after discarding 100 000 initial transients, to estimate the average velocity accurately.

The relationship between s and v_p is shown in fig. 2. If $a \gtrapprox 1.74 \approx a_{tr}$[#2] the relationship is rather

[#2] See section 8 for a_{tr}, where a possible mechanism for the change of the s–v relationship at a_{tr} is discussed.

simple. The velocity of an attractor turns out to be proportional to its asymmetry s, as is plotted in fig. 2b. Here we note that there is a gap of velocity between frozen attractors ($v_p = 0$) and traveling attractors. For an attractor with velocity $v = 0$, s is zero within numerical accuracy. Thus spatial symmetry is attained through the attraction to the non-traveling attractor, starting from an initial condition with spatial asymmetry. Again, this spatial symmetry is not a local but a global property. Indeed, for each domain over a single wavelength, its waveform is not generally mirror symmetric. The asymmetry in each wave form is cancelled through the summation over the entire lattice. This attainment of self-organized symmetry is possible under the existence of traveling attractors. Indeed, for a weaker coupling regime without a traveling attractor, all attractors have a fixed structure [5], but they are not generally spatially symmetric. Spatial asymmetry in the initial conditions is not eliminated in this case.

For $a < a_{tr} \approx 1.74$, the relationship between s and v_p is more complicated (see fig. 2a). Attractors with $v_p = 0$ can have a small non-vanishing asymmetry. The self-organized symmetry is not complete. The velocity gap between frozen attractors and moving ones is not seen. Furthermore the linear relationship between v_p and s does not hold, although we can see a band structure of velocities. One of the reasons for this complication is coexistence of attractors with different periods (or frequencies), as will be studied in the next section.

3. Phase slips: local units for global traveling wave

To understand the mechanism of this velocity selection, we note that $x_n(i)$ oscillates in time. For $\epsilon = 0.5$, the oscillation is almost periodic and the period is very close to 4. Then one can assign a phase of oscillation to a lattice site i relative to $(x_n(i), x_n(i+1))$. It is possible to assign a phase change $\frac{1}{2}m'\pi(m' = \pm 1)$ between the lattice site i and the lattice site $i+j$ in the neighboring domain, according to the order of the period-4 like motion.

When there is a phase gap of 2π between sites i and $i+l$, it is numerically found that this interval unit $[i, i+l]$ maintains the traveling wave. For example, in the attractor with velocity v_1 in fig. 1, the oscillation is close to period 4, with slow quasiperiodic modulation. For periodic boundary conditions, the total phase change should be $2k\pi$. The velocity is zero for an attractor with $k = 0$. If $k = 1$, there must be a sequence of 5 domains with phases 0, $\frac{1}{2}\pi$, π, $\frac{3}{2}\pi$, 2π for corresponding lattice sites i (fig. 1b). This unit is a phase slip of 2π. A phase slip with a negative sign is defined by the mirror-symmetric pattern of a positive one. An attractor with the velocity of the band v_k has exactly k (positive) phase slips, in other words, $2k\pi$ phase change over the total lattice. (k equals the number of positive phase slips subtracted by negative ones.) Among attractors with the same number of phase slips, there can be various configurations of domains. The velocity variance among attractors within the same band depends on this configuration.

Since a phase slip is localized in space, one might think that the movement is a local phenomenon like soliton propagation. This is not the case. In the present case, this phase slip must pull all the other regions to make them travel, changing the phases of oscillations of all lattice points. Thus all lattice points are globally influenced by a local slip. Our dynamics gives a connection between local and global dynamics. One clear manifestation of the global aspect is the additivity of velocity. In our system, the velocity of the wave is proportional to the number of phase slips. This proportionality gives a clear distinction between our dynamics and soliton-type dynamics, where, of course, the velocity of a soliton does not increase with the number of solitons present.

Phase of oscillation at each lattice point can clearly be seen with the use of spatial return maps, 2-dimensional plots of $(x_n(i), x_n(i+1))$.

When there is a phase slip, the spatial return map shows a curve as in fig. 3. A point $(x_n(i), x_n(i+1))$ rotates clockwise with time when there is a phase slip, while the point does not rotate for a non-traveling attractor. When there are two phase slips, the rotation speed is twice in addition to a slight change of the curve. We note that the motion is smooth without any remarkable change of rotation speed even when the lattice site lies at the phase slip region. In fig. 3, we have plotted spatial return maps for attractors with 1 and 4 phase slips. In the figure the system size is 64 lattice sites while each phase slip requires 16 lattice sites. Thus the attractor with 4 slips (see fig. 3b) consists only of a sequence of 4 repeated phase slip patterns. For attractors with less than 4 slips, there can be variable configurations of domains other than the phase slips. Depending on the configuration, the spatiotemporal return maps are different.

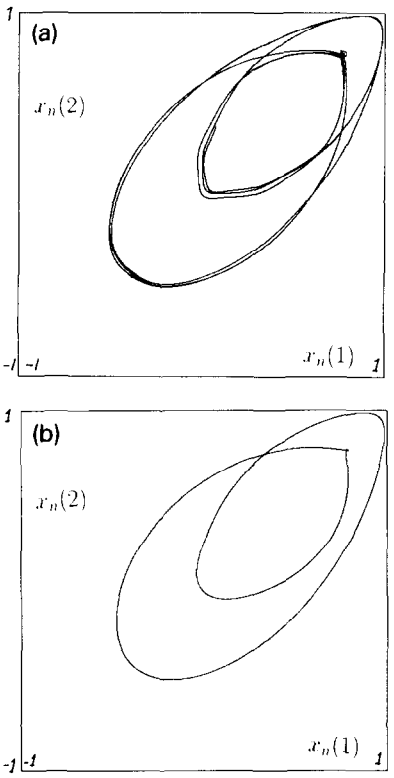

Fig. 3. Spatial return map: $\{x_n(1), x_n(2)\}$ are plotted over the time steps $n = 10\,001, 10\,002, \ldots, 21\,000$. $a = 1.70$, $\epsilon = 0.5$, and $N = 64$. (a) An attractor with one phase slip (b) an attractor with four phase slips. The return map for an attractor with three slips shows a quasiperiodic modulation, typical to a three-dimensional torus [3].

When the return map shows a closed curve, the attractor is on a projection of a 2-dimensional torus. This is the case in the state consisting only of phase slips (see fig. 3b). In general, the curve is not closed and the return map forms surface rather than a curve, suggesting a higher-dimensional attractor. Indeed, another frequency modulation is observed in the spatial return map, for the return map with two or three phase slips. As will be confirmed in section 5, the attractor is on a higher-dimensional torus. Frequencies of quasiperiodic modulation depend on the number of phase slips and the configuration of the domains.

The proportionality between the asymmetry and the velocity (see section 2) can (partially) be explained by the phase slip mechanism: Each (positive) phase slip gives rise to a certain contribution to the asymmetry s. In fig. 2b, however, the proportionality holds even in a level within each band where the number of slips is identical. The asymmetry can depend on the configurations of domains, besides the number of slips. So far it is not clear why the proportionality holds even for such small changes of the asymmetry by the configurations, when the nonlinearity is large.

4. Basin volume and parameter dependence

For random initial conditions, the probability to hit an attractor with the velocity 0 or $\pm v_1$ is rather high. We have measured the basin volume ratio for attractors of different velocities (see also fig. 3 of [1]). A band structure of admissible velocities is confirmed. In each band there are discrete sets of admissible velocities. We have confirmed that there are many attractors with different velocities within each band by running a long-time simulation.

As the velocity of an attractor increases, its basin volume shrinks rather drastically (see table 2). The basin volume for v_1 is often rather large. Basin volumes decrease (approximately) in a Gaussian form with the velocity of the band ($\exp(-K^2 \times \text{const.})$ for attractors in the band $v_p = Kv_1$). This Gaussian decrease is generally observed for any parameter value, although the basin ratios for the fixed and v_1 attractors may vary.

The above behavior of basin volumes is explained through the phase slip mechanism. Let us assume that by a random initial condition, a phase change between two domains ($\pm\frac{1}{2}\pi$) is randomly assigned. (We have to impose the constraint that its sum should be a multiple of integers of 2π, but this is not important for the following rough estimate.) Then the probability for the sum of the phase changes obeys the binomial distribution. For large N, the probability to have K phase slips is estimated as

$$\exp[-(K/\sigma)^2] \quad \text{with } \sigma \propto \sqrt{N}\,. \tag{3}$$

Thus the probability to have K phase slips is expected to decay with a Gaussian form with K. Thus the Gaussian form of the basin volume is explained.

Dependences of the velocity v_p on the parameter a and size N are given in figs. 4a,b. In these figures, we have measured the velocity by taking the average over 160 000 time steps, after discarding 800 000 transients starting from several

Table 2
Velocity, asymmetry, and basin volume of fixed and traveling attractors. $a = 1.73$, and $\epsilon = 0.5$. 500 attractors from random initial conditions are chosen to estimate the basin volume ratio.

Velocity	Asymmetry s	Basin volume ratio (%)
0	0	34.6
$\pm v_1 = 0.95 \times 10^{-3}$	2.5×10^{-5}	23.7
$\pm v_2 = 1.95 \times 10^{-3}$	5.3×10^{-5}	7.2
$\pm v_3 = 2.9 \times 10^{-3}$	8.3×10^{-5}	1.6
$\pm v_4 = 3.8 \times 10^{-3}$	12×10^{-5}	0.2

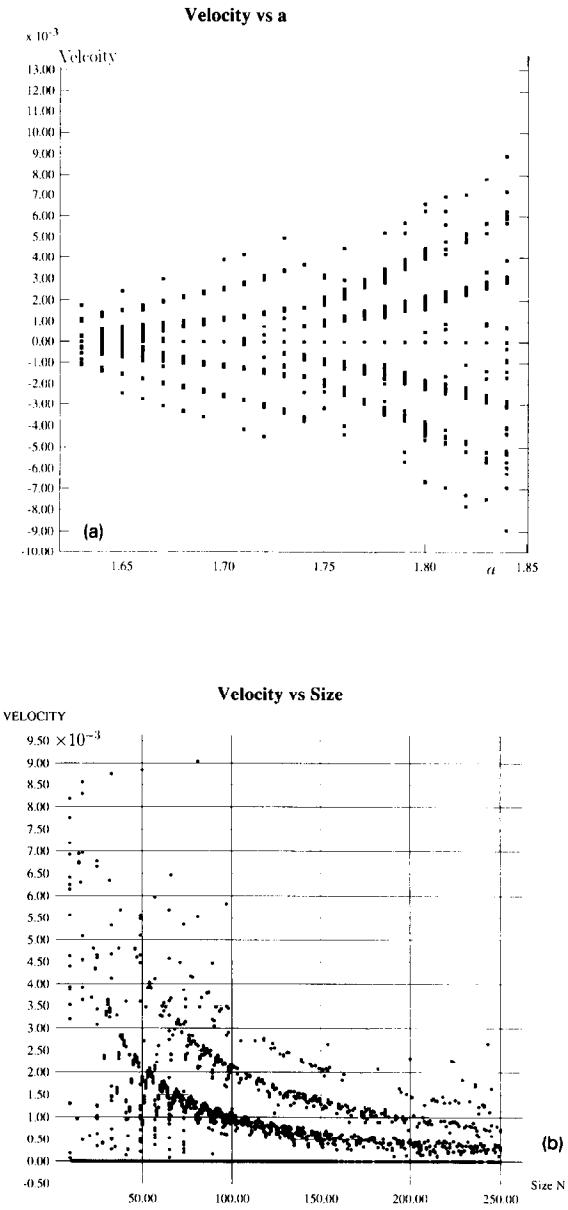

Fig. 4. Dependence of velocities of attractors on a and size N. (a) Velocities versus a; velocities from randomly chosen 100 initial conditions are overlayed, obtained with the algorithm in the text, applied per 32 steps, over 32×5000 steps, after discarding 50 000 initial transients. $N = 100$, and $\epsilon = 0.5$ (additional data are included from fig. 5 in [1]).

(b) The absolute values of velocities $|v_p|$ of attractors, plotted as a function of size N. The velocities are computed with the algorithm in the text, applied per 32 steps, over 32×5000 steps, after discarding 50 000 initial transients. Velocities from randomly chosen 50 initial conditions are overlaid. $a = 1.73$, and $\epsilon = 0.5$.

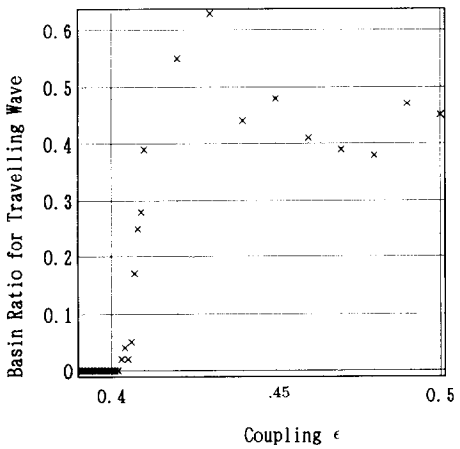

Fig. 5. Basin ratio for traveling wave as a function of ϵ, for $a = 1.69$. Velocity of attractors from randomly chosen 50 initial conditions are examined, to count the number of attractors with $v \neq 0$.

initial conditions. These averaged velocities are plotted for $1.6 < a < 1.85$ for $N = 50$ (in fig. 4a), while they are plotted over $10 < N < 250$ for $a = 1.73$, in fig. 4b. We can see the selection of discrete velocities rather well. Velocities lie in a narrow band around v_k.

As is given in fig. 5, selected velocities slowly decrease with the system size. The $1/\sqrt{N}$ dependence of the velocity (fig. 4b) is explained by the argument at eq. (3). Since our system has a selected wavelength R, the fractional part of N/R is important for the nature of traveling wave[#3], besides the above size dependence. Except for this additional dependence, the velocity decrease is roughly fitted by $1/\sqrt{N}$ up to $N = 200$. We also note that higher bands successively appear (v_k with larger k), with the increase of the system size, although the basin volume for such higher bands is rather small due to the Gaussian decay.

As has been reported, no traveling state has been observed for $\epsilon < \epsilon_c \approx 0.402$. We note that the velocity does not go to zero as ϵ approaches ϵ_c from above. For $0.402 < \epsilon < 0.45$ the velocity lies between 1.0×10^{-3} and 1.8×10^{-3} without displaying any symptoms of a decrease. Rather, the basin volume for the traveling attractor vanishes with $\epsilon \to \epsilon_c$, which is the reason why only non-traveling attractors are observed for $\epsilon < \epsilon_c$. The basin volume for traveling states (i.e., all attractors with non-zero velocities) is shown in fig. 5.

[#3] See section 5 for a novel dynamical state which appears when there is a mismatch between the size and the wavelength.

5. Chaos and quasiperiodicity in the traveling wave

To examine the dynamics of our attractors, Lyapunov spectra have been measured numerically through the product of Jacobi matrices [4]. For most parameters ($1.65 < a < 2.0$) and sizes, the maximal exponent is zero, irrespective of the velocity of attractors. Thus chaos is completely eliminated by pattern selection, and the attractor is a torus. As is expected from the spatial return maps, the attractor can be a higher-dimensional torus with more than one null exponent. Between attractors with $v = 0$ and $v = v_p$, there are only slight differences in Lyapunov spectra.

In our model a (traveling) pattern is selected such that it eliminates chaos (almost) completely. If chaos were not sufficiently eliminated, it would be impossible to sustain a spatially periodic pattern during the course of propagation. Such elimination of chaos is not possible for every wave pattern, since our dynamics has topological chaos. In our system a wavelength R is selected. When the size N is not close to a multiple of the selected wavelength R, there can remain some frustration in any pattern configuration, and weak chaos can be observed.

In narrow parameter regimes, we have found chaotic traveling waves for some sizes. For example, very weak chaos is observed around $a \approx 1.70$, if N is large, as is shown in fig. 6a. The corresponding spatial return map (see fig. 6b)

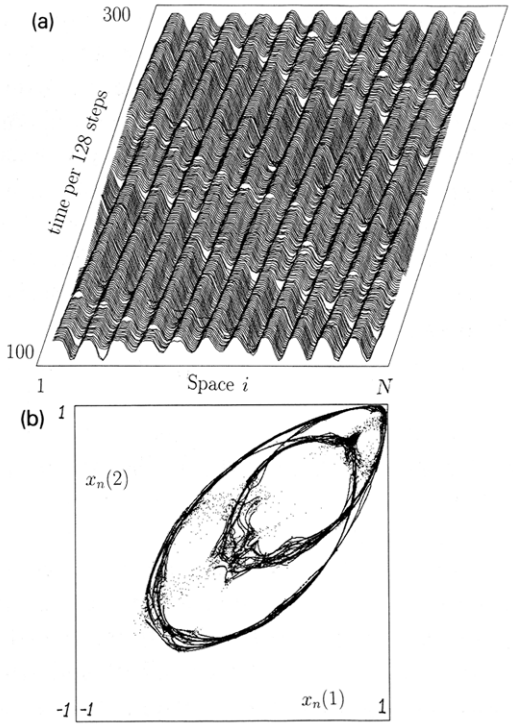

Fig. 6. (a) Amplitude–space plot of $x_n(i)$ with a shift of time steps. 200 sequential patterns $x_n(i)$ are displayed with time (per 128 time steps), after discarding 10 240 initial transients, starting from a random initial condition. $a = 1.69$, $\epsilon = 0.5$, and $N = 92$. (b) Spatial return map: $\{x_n(1), x_n(2)\}$ are plotted over the time steps $n = 10\,001$, $10\,002, \ldots, 210\,000$. $a = 1.69$, $\epsilon = 0.5$, and $N = 100$.

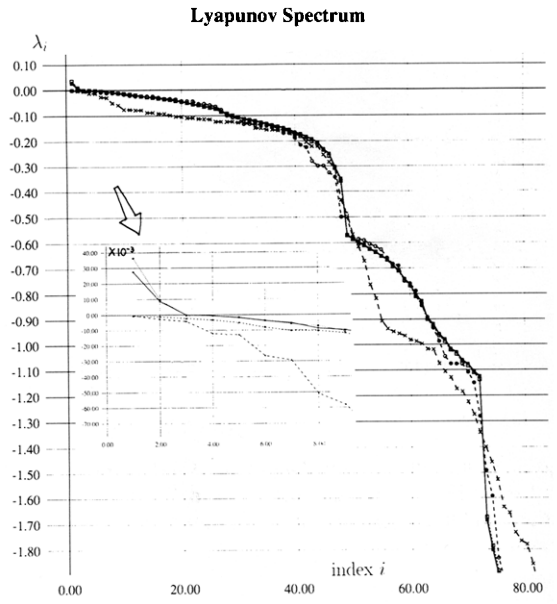

Fig. 7. Lyapunov spectra of our model with $\epsilon = 0.5$, starting with a random initial condition, discarding 50 000 initial transients. The calculation is carried out through the product of Jacobi matrices over 32 768 time steps. $N = 100$, a = 1.69: for attractors with $v = v_1$ (solid or dotted line) and $v = 0$ (broken line).

consists of curves (corresponding to regular traveling) and scattered points (corresponding to chaotic modulation). It should be noted that the chaotic modulation propagates in the opposite direction to the traveling wave. There are few positive exponents in the Lyapunov spectra for the traveling wave attractor (see fig. 7). The number of positive exponents is small (1–3) compared with the system size N. Chaos, localized in a domain, propagates as a modulation of the wave, as is shown in fig. 6a. We also note that the spectrum (see fig. 7) is almost flat near $\lambda \approx 0$. The propagating wave leads to a Goldstone mode giving rise to a null exponent.

6. Chaotic itinerancy of traveling waves

As is shown in the previous section, there remains some frustration in forming a wave pattern if the ratio N/R is far from an integer. When the frustration due to this mismatch between the size and wavelength is large, it leads to spontaneous switching among patterns (see fig. 8a). This spontaneous switching arises from chaotic motion of each pattern, and may be regarded as a novel class of chaotic itinerancy [15]. Global interaction is believed to be necessary to obtain chaotic itinerancy [15]. Although the interaction of our model is local, the phase slip globally influences all the lattice points, and thus satisfies the condition for chaotic itinerancy.

Only few remnants of curves (corresponding to the traveling structure) can be seen in the spatial return map (see fig. 8b), while scattered parts are

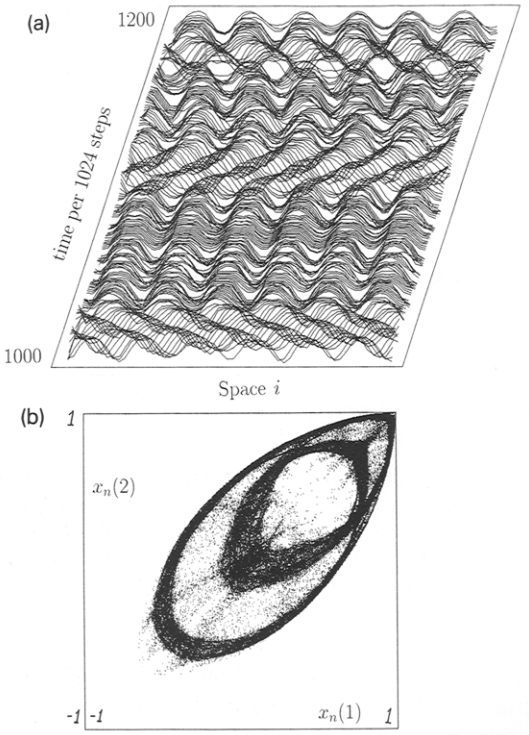

Fig. 8. (a) Amplitude–space plot of $x_n(i)$ with a shift of time steps. 200 sequential patterns $x_n(i)$ are displayed with time (per 1024 time steps), after discarding 1 024 000 initial transients, starting from a random initial condition. $a = 1.69$, $\epsilon = 0.5$, and $N = 51$. (b) Spatial return map: $\{x_n(1), x_n(2)\}$ are plotted over the time steps $n = 10\,001,\ 10\,002, \ldots,$ 210 000. $a = 1.69$, $\epsilon = 0.5$, and $N = 51$.

more dominant than in the chaotic traveling in the previous section. The direction of rotation also changes with time, through the scattered points. Both amplitudes and phases of oscillations are modulated strongly here.

For the spontaneous switching, we need some kind of modulation of the wave. Indeed, each waveform starts to be rather irregular in space and time in advance to the switching. The wavelength, on the other hand, is not affected by the course of this switching process. In general, there can be three types of modulation of the wave; frequency, phase, and amplitude modulations. In our example, frequency is hardly modulated (as is seen in the invariance of wavelength through the switching), while the phase modulation (following the amplitude one) is essential to the spontaneous switch of traveling states.

The switching occurs through the creation or destruction of a phase slip. Frustration in a pattern leads to the distortion of a phase slip, inducing chaotic motion. This chaotic motion breaks the phase slip. On the other hand, there can be the creation of a slip by chaotic modulation of the phase of oscillation. This creation or destruction of a phase slip is a local process, but influences globally the velocity of the traveling wave.

In chaotic itinerancy, long time residence at a quasi-stable state is often noted. We have measured the residence time distribution of a state with a given velocity. As is shown in fig. 9, all the residence time distributions $P_k(t)$ of a k-phase-slip state (for $k = 0, \pm 1, \pm 2$; i.e., $v_p = 0$, $v_p = \pm v_1$, $v_p = \pm 2v_1$) obey the power law $P_k(t) \approx t^{-\alpha}$ with $\alpha \approx 1$. This power-law dependence clearly indicates the long time residence at each traveling state. Similar power-law dependence of a quasi-stable state has already been found for spatiotemporal intermittency in a CML [5], although the power itself is clearly distinct.

Lyapunov spectra for this frustration-induced chaos are shown in fig. 10. The number of positive exponents is again very few (3 in the figure), whose magnitudes are very small. The chaos by the frustration is very weak and low-dimensional. The spectra have a plateau at the null exponent, implying the existence of a Goldstone mode by traveling wave. As seen in the previous section the accumulation at null exponent is characteristic of a (chaotic) system with a traveling wave.

For larger system sizes, chaotic itinerancy of waves is hardly observed. The system settles down to a frozen or traveling pattern after transients. Since the number of chaotic modes is few ($\mathcal{O}(1)$), the frustration per degree of freedom is thought to decrease with N. The distortion due to the mismatch of phases is still there, but it is distributed over a large size and is too weak to switch the pattern. The remnant frustration in a

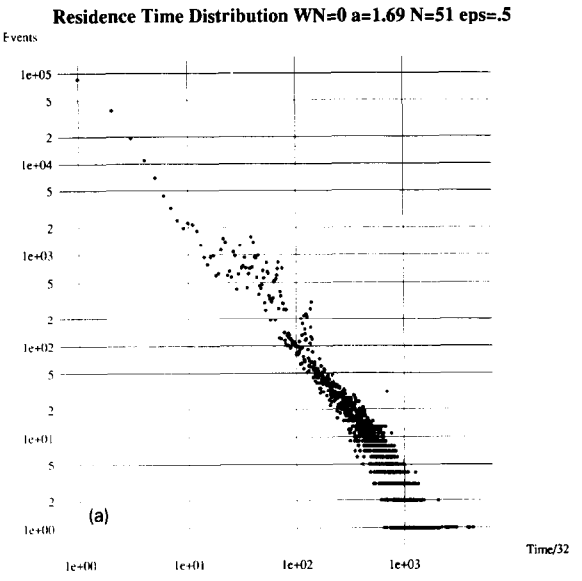

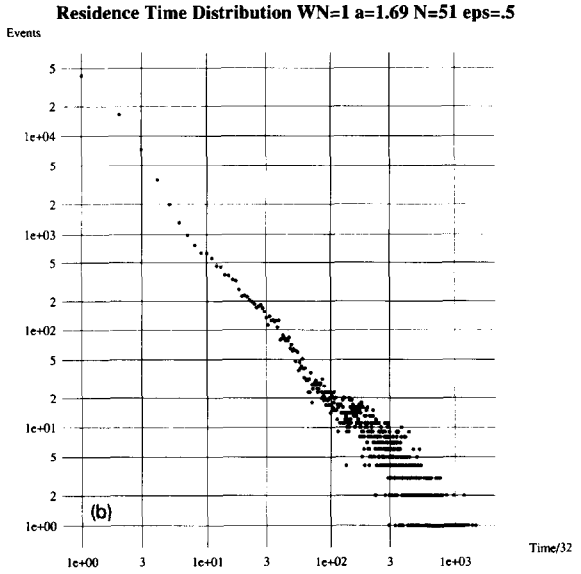

Fig. 9. Residence time distribution for a state with $v \approx v_k$ in the chaotic itinerancy of traveling wave. The distribution is taken over 819 200 time steps after 20 000 initial transients, and sampled over 500 initial conditions. $a = 1.69$, $\epsilon = 0.5$, and $N = 51$. Here the residence time distributions at the state $k = 0$ (non-traveling state), and $k = 1$ (residence at a one-phase-slip state) is plotted. The distributions at the state $k = -1$ (residence at a one-negative-phase-slip-state) and $k = 2$ (residence at a two-phase slip state) are also computed. They obey the same power law distribution as in the present figure.

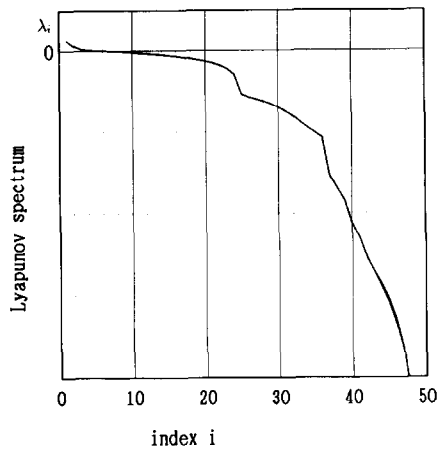

Fig. 10. Lyapunov spectra of our model with $\epsilon = 0.5$, starting with a random initial condition, discarding 50 000 initial transients. The calculation is carried out through the products of Jacobi matrices over 32 768 time steps. $N = 51$, $a = 1.69$: Spectra from three different initial conditions are overlaid.

traveling wave leads to chaotic modulation of wave as is studied in section 5.

7. Co-moving mutual information flow

Co-moving mutual information is often useful for measuring correlations in space and time [4]. From the joint probability $P(x_n(i), x_{n+m}(i+j))$, we have calculated the mutual information

$$I(m, j) = \int \mathrm{d}x_n(i)\, \mathrm{d}x_{n+m}(i+j) \times P(x_n(i), x_{n+m}(i+j)) \times \log \frac{P(x_n(i), x_{n+m}(i+j))}{P(x_n(i))\, P(x_{n+m}(i+j))} . \quad (4)$$

In a traveling wave, we have peaks in $I(m, j)$ at $I(t, v_p t)$ for an attractor traveling with v_p. For a quasiperiodic attractor the peak height does not decay with the time delay t, while it slowly decays for a chaotic attractor. The transmission of correlations can clearly be seen.

In a chaotic attractor, however, there is also propagation of small modulations on the travel-

ing wave. This propagation is in the opposite direction to the wave. From the above mutual information, this reverse propagation could not easily be measured so far. The propagation of chaotic modulation implies the flow of information created by chaos [18]. One way to measure this information creation may be the use of three point mutual information with the use of $P(x_n(i), x_{n+m}(i+j), x_{n+m+l}(i+j))$ [19], while another possible way of characterizing a chaotic traveling wave is the use of the co-moving Lyapunov exponent [4]. A slight increase of the exponent at the traveling velocity is observed. In our case, however, chaos is too weak to give a quantitative distinction.

The mutual information in the chaotic itinerancy decays with time and space, without any peaks at some velocity. By the switching process, all local traveling structures are smeared out, leading to the destruction of peaks in the mutual information at some velocities.

8. Chaotic transients before the formation of traveling waves

To fall on a traveling (or fixed) attractor, the velocities of all local domains of unit wavelength must coincide. Thus it is expected that the transient time before falling on an attractor may increase with the system size. As for the transient behavior, our transient wave phase splits into the following two regimes.

(i) For the medium nonlinearity regime ($a < a_{tr} \approx 1.74$), the transient length increases at most with the power of N. Indeed, local traveling wave patterns are formed within a few time steps. Before hitting the final attractor, these local waves are slightly modulated to form a global consistency. The formation of a global wave structure occurs for time steps smaller than $\mathcal{O}(N)$. We need time steps in the order of $\mathcal{O}(N)$ for the slight modulation to adjust the phases of all domains. (See fig. 11a for the spacetime diagram.)

(ii) For larger nonlinearity ($a > a_{tr}$), there are long-lived chaotic transients before our system falls on a traveling-wave attractor. The transient length increases with the system size rather rapidly: the increase is roughly estimated by $\exp(\text{const.} \times N)$ [16], although some (number-theoretically) irregular variation remains. In the transient process, the dynamics is strongly chaotic, and is attributed to "fully developed

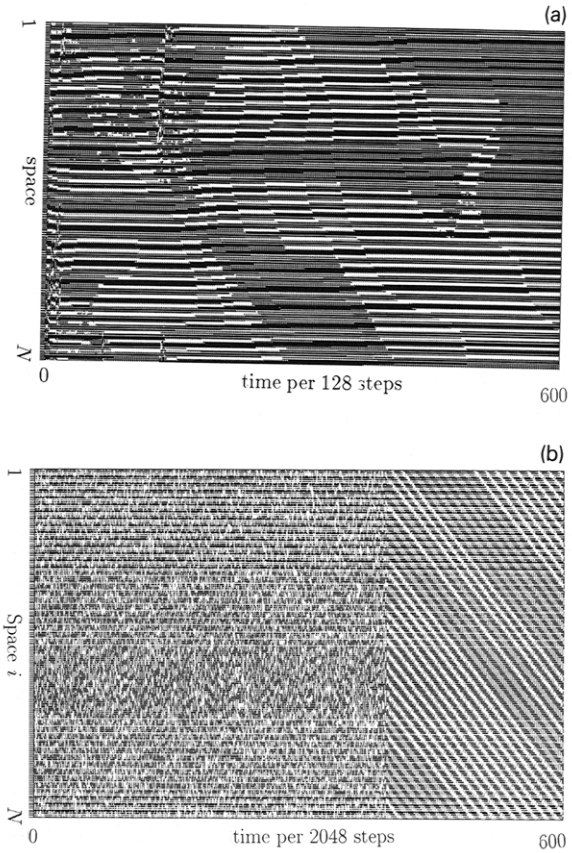

Fig. 11. Spacetime diagram for the coupled logistic lattice (1), with $\epsilon = 0.5$, and starting with a random initial condition. If $x_n(i)$ is larger than x^* (unstable fixed point of the logistic map), the corresponding spacetime pixel is painted as black (if $x > x_2^* = (\sqrt{1+7a} - 1)/2a$ painted darker), while it is left blank otherwise. (a) $a = 1.71$, $N = 300$. Every 128th step is plotted. (b) $a = 1.76$, $N = 200$. Every 2048th step is plotted.

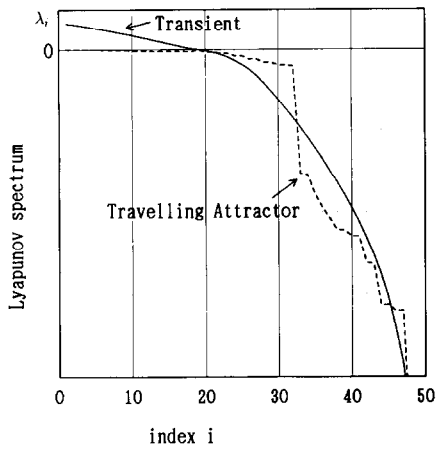

Fig. 12. Lyapunov spectra of our model with $\epsilon = 0.5$, starting with a random initial condition: Comparison of quasistationary states with an attractor. In the former, two sets of spectra in the transients states are calculated after discarding 10 000 initial transients, for two different initial conditions. They are overlaid, but agree within the linewidth of the figure. For the latter, the data after 1 000 000 steps are adopted. The calculation is carried out through the products of Jacobi matrices over 32 768 time steps. $N = 50$, $a = 1.88$.

spatiotemporal chaos" in [5][#4]. Lyapunov spectra during the transients are shown in fig. 12, in contrast with the spectra of an attractor. This transient process is quasistationary (see fig. 11b for the spacetime diagram); No gradual decay is observed for dynamical quantifiers such as the short-time Lyapunov exponent [13] or Kolmogorov–Sinai entropy. Such dynamical quantifiers fluctuate around some positive value, till a sudden decrease occurs at the attraction to the regular attractor. These observations are consistent with the type-II supertransients often observed in spatially extended systems [12]. In a strong coupling regime, we have found traveling wave states up to the maximal nonlinearity $a = 2$. Thus the fully developed spatiotemporal chaos in this regime may belong to supertransients [16].

We note that the linear relationship between the asymmetry s and the velocity v (in section 2) is seen only for $a > a_{tr}$. This relationship may be partially explained from the results in the present section, although further studies are necessary for a complete explanation: For $a < a_{tr}$, the pattern selection can occur locally, and some local distortion in the wave pattern may not be removed. Then spatial asymmetry can remain even for a non-traveling attractor, and the s–v relationship can be very complicated. For $a > a_{tr}$, on the other hand, slight distortion in wave pattern leads to global chaotic transients. Only patterns without distortion are admissible as attractors. The s–v relationship may be expected to be monotonic and simpler.

[#4] If a is not so large (near $a \approx a_{tr}$), we have often observed some local traveling wave patterns during the transients. The dynamics here can be attributed to the spatiotemporal intermittency of type-II [9–11].

9. Switching among attractors with different velocities

By a suitable input at a site at one time step, we can make an external switch from one attractor to another (with a different velocity). By a local input, the structure of an attractor is changed over the whole lattice. Local information by an input is transformed into a *global* wave pattern. In the medium nonlinearity regime ($a < a_{tr}$), the switching process occurs within a short time, without any global chaotic transients.

As is expected this switching is easily attained by applying an input at site(s) in a phase slip. For example, assume that the phases at neighboring 5 domains are given by $[0, +\frac{1}{2}\pi, +\pi, +\frac{3}{2}\pi, 2\pi]$. By applying an input at site(s) of the third domain, the phases can be switched to $[0, +\frac{1}{2}\pi, 0, -\frac{1}{2}\pi(=\frac{3}{2}\pi), 0]$. Thus a phase slip is removed, leading to a switch to an attractor with $v \to v_{next} \approx v - v_1$. We can control a switch by choosing an input site and value so that the number of phase slips is in(de)creased.

For larger nonlinearity ($a > a_{tr}$), the chaotic transient lasts for many time steps during the course of switching. In this case the control of switching is almost impossible; it is hard to

predict the length of the switching process or the attractor after the switch. This type of chaotic transients in the search for an attractor can be seen in some models with chaotic itinerancy [15] and in the neural activity in an olfactory bulb [17].

10. Wandering domain by chaos

In the weak coupling case, a frozen random pattern is observed [5] for weak nonlinearity ($a < 1.55$). In our strong coupling regime, domains with variable sizes are again formed. These domains, however, are not fixed in space. The boundary of domains here fluctuates in time. A region can move in one direction locally, but then it changes the direction of traveling (see fig. 13a). In spatial return maps, the motion of $(x_n(i), x_n(i+1))$ along a curve changes its direction with time (see fig. 14). The boundary motion is diffusive and Brownian-like (see fig. 13). Furthermore, the size of domains can also vary (chaotically). Domain distribution is rather random. We have plotted the spatial power spectrum $S(k) = \langle |\Sigma_j x_n(j) \exp(ikj)|^2 \rangle$ with the temporal average $\langle \cdots \rangle$. In contrast with the peaks corresponding to the selected wavelength in the regular traveling wave regime, there are no clear peaks in the spectra. The decay of the power spectra with the wavenumber k is consistent with the diffusive motion of domains, while the decay in the frozen random phase in the weak coupling regime is much slower, due to the absence of such diffusive motion.

In this phase, some attractors have phase slips. Again a phase slip is defined by a unit with a sequence of domains of 2π phase advance. In an attractor with phase slips, the pattern moves (in average) in one direction with some fluctuation. Generally the pattern has some average velocity depending on the number of phase slips, although a fluctuating boundary of domains brings about the fluctuation of the velocity. Here chaos is not eliminated in large domains. In this case

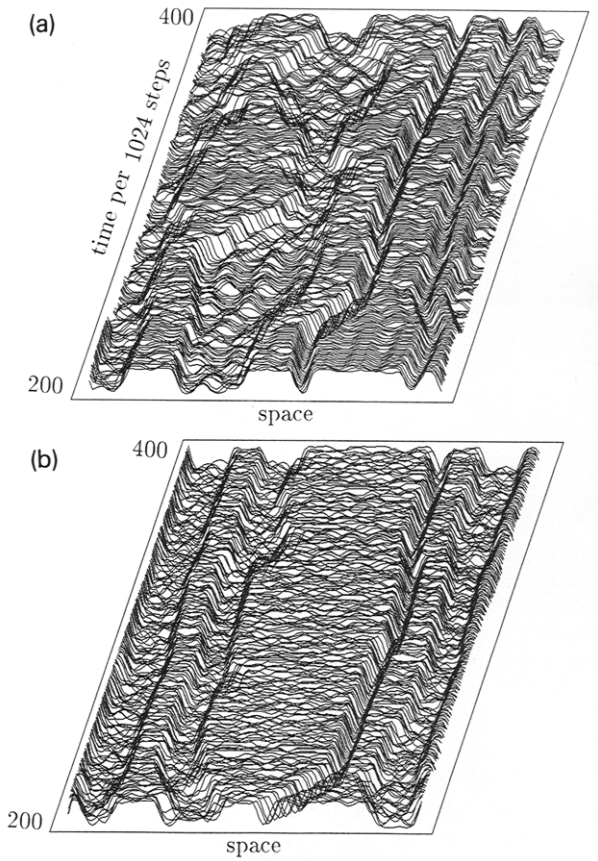

Fig. 13. Amplitude–space plot of $x_n(i)$ with a shift of time steps. 200 sequential patterns $x_n(i)$ are plotted with time (per 1024 time steps), after discarding 20 480 initial transients, starting from a random initial condition. $\epsilon = 0.5$, and $N = 100$. (a) $a = 1.47$, (b) $a = 1.52$.

chaos is transported along with the traveling wave. Chaos localized in large domains moves together with the wave and in the same direction. An example of a pattern is given in fig. 14b with the corresponding spatial return maps.

If a is smaller, domains of various sizes coexist, while the appearance of larger domains is less frequent as a approaches ≈ 1.55, where pattern selection sets in.

Chaos in the internal dynamics in a large domain is confirmed by the Lyapunov spectra given in fig. 15. The slope of the spectra is small at $\lambda \approx 0$. These exponents near 0 are thought to

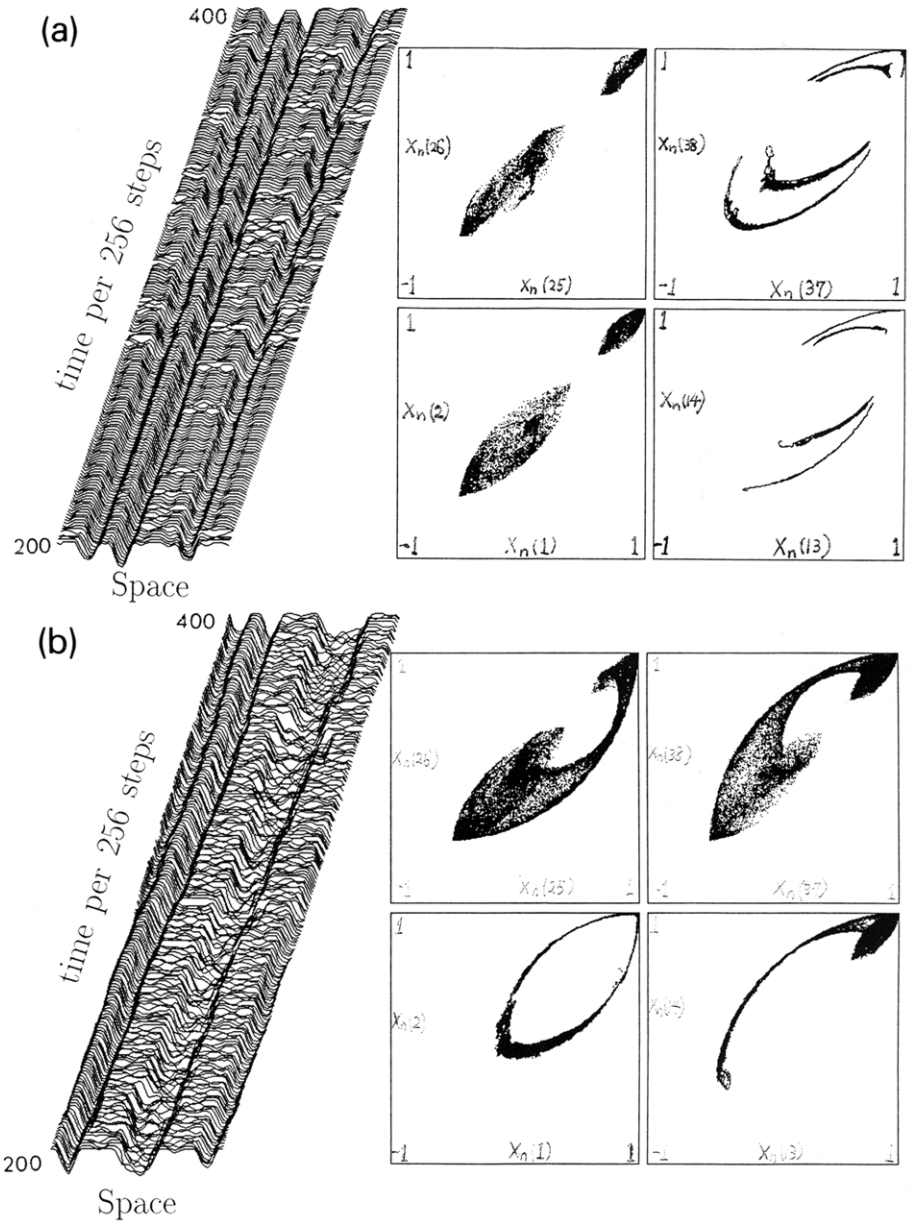

Fig. 14. Spatial return maps with the corresponding space amplitude plots: $(x_n(1), x_n(2))$, $(x_n(13), x_n(14))$, $(x_n(25), x_n(26))$, and $(x_n(37), x_n(38))$ are plotted over the time steps $n = 12\,800, 12\,801, \ldots, 64\,000$, while $x_n(i)$ is plotted with time per 256 steps. $a = 1.5$, $\epsilon = 0.5$, and $N = 50$; (a) without any phase slip. (b) With one phase slip.

come from the diffusive motion of the domains. Co-moving mutual information decays exponentially in space and time, implying that there are no remaining patterns in space and time.

11. Propagating kinks in period-doubling media

To clarify the difference between the phase slips and conventional solitons, we have studied

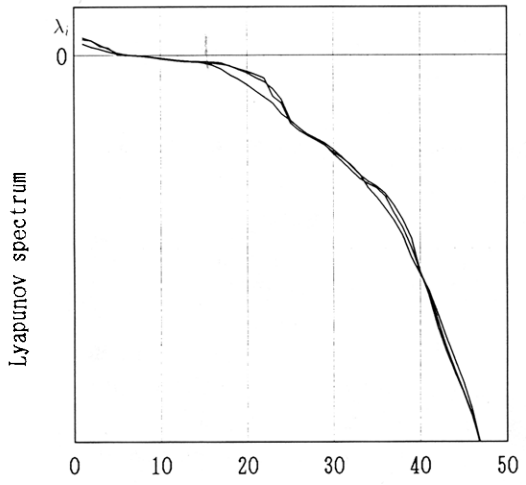

Fig. 15. Lyapunov spectra of our model with $\epsilon = 0.5$, starting with a random initial condition. Three examples of calculation are overlaid starting from 3 randomly chosen initial conditions, after discarding 10 000 initial transients. Calculated over 32 768 time steps. $N = 50$, $a = 1.53$.

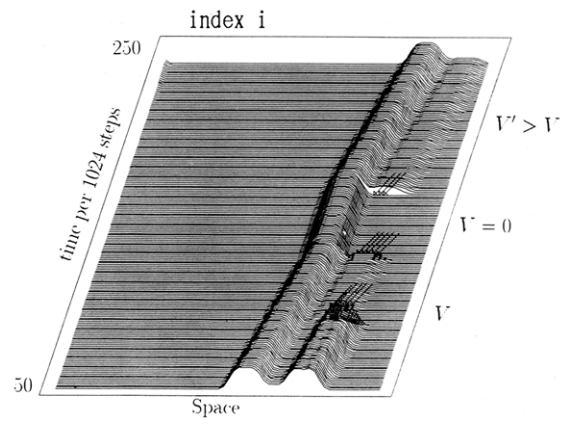

Fig. 16. Amplitude–space plot of $x_n(i)$ (for a moving kink) with a shift of time steps. 200 sequential patterns $x_n(i)$ are depicted with time (per 1024 time steps), after discarding 4096 initial transients, starting from a random initial condition. At the time steps and lattice points indicated by the arrows, the value of $x_n(i)$ at the corresponding i and n shifted to 0 by an input. $a = 1.4$, $\epsilon = 0.5$, and $N = 64$.

our CML in the period-doubling regime with a strong coupling. As is known our CML exhibits the period-doubling of kink patterns [2]. In the lower coupling regime ($\epsilon < 0.4$), these kinks are pinned at their positions. In the strong coupling regime, some kinks can move when they form a phase gradient in one direction (see for example fig. 16). This phase in-(de-)crease is possible if the period of the kinks is larger than 2.[#5] If the period is 4, for example, there can be a series of domains with the increase of the phase $0, \frac{1}{2}\pi, \frac{3}{2}\pi, 2\pi$, separated by 3 kinks. These kink patterns form a phase gradient, which drives them to move with a constant speed.

As for this phase advance, these moving kinks are similar to our phase slips. However, the kinks here are completely local. When there are two kinks at a distant position, they move almost independently with their original speeds, (until they collide). See fig. 16, where elimination of one kink by external input does not cause any change to the propagation of the other kink. Furthermore, there is no discrete selection of speeds. The speed of a kink gradually varies with the phase gradient within the kink pattern. In fig. 16, change of a tail width at a kink leads to a slight change of speed.

The local propagation and the shape dependence of speed imply that the mechanism of kink propagation here is essentially same as that (usually) studied in partial differential equations like a ϕ^4 system. In table 3 the differences between the kink here and the traveling wave by phase slips are summarized. In an oscillatory medium (without chaos), we can expect the existence of kinks with period-doubling as in the present example.

12. Summary and discussions

In the present paper we have reported a traveling wave triggered by phase slips. The velocity of traveling attractors forms quantized bands determined by the number of phase slips.

[#5] This type of moving kink domains is first discussed in [20]. In the case of a period-2 attractor, possible attributed phases are π or $-\pi$. Thus it is impossible to distinguish between the phase increase or decrease (for example, the phase changes with the sequence of $\pi, -\pi, \pi$ can have neither phase advance nor retardation).

Table 3
Traveling wave by phase slips vs kinks in period-doubling media.

	Traveling wave	Kink propagation
Local unit	phase slip	kink
Range of a	$1.55 < a < 2.0$	$1.25 < a < 1.401\ldots$
Mechanism	global	local
Velocity	proportional to no. of phase slips	varies with the kink shape (tail width)
Underlying structure	spatially periodic	spatially homogeneous

Frozen attractors (without any phase slips) and traveling attractors with different velocities coexist. The velocity of each band increases linearly with the number of slips. When the nonlinearity is large, the proportionality between the asymmetry of a pattern and the velocity holds even within each band. In this case, (approximate) symmetry is self-organized for frozen attractors. See table 1 in section 1 for the phase diagram of our CML model in a strong coupling regime.

Through pattern selection of domains with some wavenumbers, chaos is completely eliminated leading to quasiperiodicity. When there is a mismatch between the size and the wavelength, remaining frustration leads to a chaotic motion of the wave. If the frustration is large, chaotic itinerancy over many traveling (and frozen) states is observed. Our system makes itinerancy over states with different velocities of traveling. The residence time in each state obeys a power law distribution. If the frustration is not so large, a chaotic traveling wave is observed, where the chaotic modulation is transmitted in the opposite direction to traveling wave.

It should be noted that a local phase slip affects globally the motion of the total system. This is in strong contrast with the kink type propagation (also observed in our system in a non-chaotic region), where it propagates as a local quantity. The additivity of velocity of the wave with the number of phase slips is a clear manifestation of the global nature.

By local external inputs, one can create or destroy a phase slip, and to switch to an attractor with a different velocity. By the traveling wave, information is transmitted to the whole space within the steps in the order of $\mathcal{O}(N)$. Thus the transformation from local to global information is possible through this switching, which may be useful for information processing and control.

We have noted two types of transient processes in the course of attraction to traveling states. When the parameter for the nonlinearity is large, a supertransient (with quasistationary measure) is observed whose transient length increases exponentially with the system size, while such rapid increase is not seen in the medium nonlinearity regime ($a < 1.75$).

In the weaker nonlinearity regime ($a < 1.55$) corresponding to the frozen random phase, we have found fluctuation of domain sizes and Brownian-like motion of domains. Coexistence of fluctuating domains and phase slips is also noted. In this random pattern, chaos is localized in large domains, and propagates along the traveling wave.

We have analyzed the dynamics of the traveling wave with the use of spatial return maps, Lyapunov spectra, and co-moving mutual information flow. When chaos is suppressed in the pattern selection regime, the maximal Lyapunov exponent is zero implying that the traveling wave attractor is on a torus whose dimension depends on the number of phase slips. This null Lyapunov exponent remains even in a chaotic wave or chaotic itinerancy. This exponent is due to the Goldstone-type mode corresponding to the traveling structure. Through the mutual information flow, we note the creation and

transmission of information by a chaotic traveling wave. The chaotic modulation added on the traveling wave leads to the possibility of information transmission, created by chaos [18].

There is no a priori reason to deny the possibility of the global traveling wave by a local phase slip, in partial differential equation systems. For convenience of an illustration, consider a partial differential equation with two components

$$\frac{\partial \boldsymbol{\phi}(r,t)}{\partial t} = \boldsymbol{F}(\boldsymbol{\phi}(r,t)) + D\,\nabla^2 \boldsymbol{\phi}(r,t)\,. \tag{5}$$

If there exists a constant velocity traveling wave solution $\boldsymbol{\phi}(r,t) = \boldsymbol{f}(r - vt)$, it must satisfy

$$-v\boldsymbol{f}' = \boldsymbol{F}(\boldsymbol{f}) + D\boldsymbol{f}''\,. \tag{6}$$

If this coupled second order differential equation has a periodic solution for a range of velocities v, then the traveling wave $\boldsymbol{f}(r - vt)$ can be a solution of eq. (5). Generally speaking, the nonlinear equation (6) has a chaotic solution for some range of v, and has windows of limit cycles in the parameter space (v) for chaos. A stable traveling wave is possible if chaos is eliminated by the choice of v. This scenario implies the existence of admissible velocity bands for stable traveling wave solutions, as in our CML example.

Traveling waves have often been studied in various experiments [21]. Quite recently, Croquette's group has observed traveling waves in Bénard convection with periodic boundary condition. Indeed this traveling wave is triggered by a unit of a 2π phase advance [23]. They have also observed chaotic itinerancy over different traveling states, when the motion in a Bénard cell is strongly chaotic [24]. It is expected that this discovery belongs to the same class as our traveling wave. It is interesting to check if attractors with different velocities coexist by applying perturbations to such experimental systems. A search for our velocity bands in experiments will also be of interest. Detailed comparison with our model and experiments will be important in future.

In the weak nonlinearity regime, the suppression of chaos is not possible, where domains show chaotic Brownian motion without a traveling velocity. This type of floating domains has some correspondence with the dispersive chaos found in Bénard convection by Kolodner's group[#6].

Acknowledgements

I would like to thank K. Nemoto, Frederick Willeboordse, K. Ikeda, M. Sano, S. Adachi, T. Konishi, J. Suzuki, for illuminating discussions. This work is partially supported by Grant-in-Aids (No. 04231102) for Scientific Research from the Ministry of Education, Science and Culture of Japan. A preliminary version of the paper was completed in February of 1992, although I have had many fruitful discussions since then. I would like to thank again Frederick Willeboordse for discussions, critical comments to the manuscript, and for sending me his Doctoral thesis in advance. My stay at Paris in June 1992 gave me an exciting chance to encounter a beautiful experiment by Croquette's group. I am grateful to Hugues Chaté for his hospitality during my stay and discussions. This travel was supported by Grant-in-Aids (no. 04044020) for Scientific Research from the Ministry of Education, Science and Culture of Japan.

References

[1] Rapid communication of the present studies is given in K. Kaneko, Phys. Rev. Lett. 69 (1992) 905.
[2] K. Kaneko, Prog. Theor. Phys. 72 (1984) 480; 74 (1985) 1033.
[3] K. Kaneko, Collapse of Tori and Genesis of Chaos in

[#6] Yanagita has recently observed the traveling wave in Bénard convection in the CML model for convection [24].

Dissipative Systems, Ph.D. Thesis (1983) (enlarged version is published by World Scientific, 1986).
[4] K. Kaneko, Physica D 23 (1986) 436.
[5] K. Kaneko, Physica D 34 (1989) 1; D 36 (1989) 60.
[6] J.P. Crutchfield and K. Kaneko, Phenomenology of Spatiotemporal Chaos, in: Directions in Chaos (World Scientific, 1987).
[7] K. Kaneko, Simulating Physics with Coupled Map Lattices – Pattern Dynamics, Information Flow, and Thermodynamics of Spatiotemporal Chaos, in: Formation, Dynamics, and Statistics of Patterns, eds. K. Kawasaki, A. Onuki and M. Suzuki (World Scientific, 1990).
[8] I. Waller and R. Kapral, Phys. Rev. A 30 (1984) 2047; R. Kapral, Phys. Rev. A 31 (1985) 3868.
[9] H. Chaté and P. Manneville, Physica D 32 (1988) 409.
[10] J.D. Keeler and J.D. Farmer, Physica D 23 (1986) 413; [5].
[11] P. Grassberger and T. Schreiber, Physica D 50 (1991) 177.
[12] J.P. Crutchfield and K. Kaneko, Phys. Rev. Lett. 60 (1988) 2715;
K. Kaneko, Phys. Lett. A 149 (1990) 105.
[13] K. Kaneko, Prog. Theor. Phys. Suppl. 99 (1989) 263.
[14] R.J. Deissler and K. Kaneko, Phys. Lett. A 119 (1987) 397.
[15] K. Kaneko, Phys. Rev. Lett. 63 (1989) 219; Physica D 41 (1990) 38;
K. Ikeda, K. Matsumoto and K. Ohtsuka, Prog. Theor. Phys. Suppl. 99 (1989) 295;
I. Tsuda, in: Neurocomputers and Attention, eds. A.V. Holden and V.I. Kryukov (Manchester Univ. Press, 1990).
[16] F. Willeboordse, Phys. Rev. E (Brief Reports), in press (1992); Ph.D. Thesis, Tsukuba University, to be submitted.
[17] W. Freeman and C.A. Skarda, Brain Res. Rev. 10 (1985) 147;
W. Freeman, Brain Res. Rev. 11 (1986) 259.
[18] R. Shaw, Z. Naturforsch. 36a (1981) 80; The Dripping Faucet as a Model Chaotic System (Aerial Press, Santa Cruz, 1984).
[19] K. Ikeda and K. Matsumoto, Phys. Rev. Lett. 62 (1989) 2265.
[20] C. Bennett, G. Grinstein, Y. He, C. Jayaprakash and D. Mukamel, Phys. Rev. A 41 (1990) 1932.
[21] D.R. Ohlsen et al., Phys. Rev. Lett. 65 (1990) 1431;
P. Kolodner, Phys. Rev. A 42 (1990) 2475;
V. Croquette and H. Williams, Physica D 37 (1989) 295;
D. Bensimon et al., J. Fluid Mech. 217 (1990) 441.
[22] P. Kolodner, J.A. Glazier and H. Williams, Phys. Rev. Lett. 65 (1990) 1579.
[23] V. Croquette, J.M. Flesselles and S. Jucquois, private communication.
[24] T. Yanagita and K. Kaneko, Phys. Lett. A 175 (1993) 415.